The British Journal of Radiology, 76 (2003), 631–637 © 2003 The British Institute of Radiology
DOI: 10.1259/bjr/69317841

High resolution MRI of the brain at 4.7 Tesla using fast spin echo imaging

[1]E DE VITA, Laurea, MS, [1]D L THOMAS, PhD, [2]S ROBERTS, PhD, [1]H G PARKES, PhD, [1]R TURNER, PhD, [1]P KINCHESH, PhD, [1]K SHMUELI, MSc, [3]T A YOUSRY, MD and [1]R J ORDIDGE, PhD

[1]*The Wellcome Trust High Field MR Research Laboratory, Department of Medical Physics and Bioengineering, University College London, 12 Queen Square, London WC1N 3AR,* [2]*MR Research Systems, Unit 5, Merrow Lane, Guildford, Surrey GU4 7BF and* [3]*Division of Neuroradiology, Institute of Neurology, Queen Square, London WC1N 3BG, UK*

Abstract. Over recent years, high field MR scanners (3 T and above) have become increasingly widespread due to potential advantages such as higher signal-to-noise ratio. However, few examples of high resolution images covering the whole brain in reasonable acquisition times have been published to date and none have used fast spin echo (FSE), a sequence commonly employed for the acquisition of T_2 weighted images at 1.5 T. This is mostly due to the increased technical challenges associated with uniform signal generation and the increasingly restrictive constraints of current safety guidelines at high field. We investigated 10 volunteers using an FSE sequence optimized to the 4.7 T environment. This sequence allows the acquisition of 17- and 34-slice data sets with an in-plane resolution of approximately 500 μm × 500 μm and a slice thickness of 2 mm, in 5 min 40 s and 11 min 20 s, respectively. The images appear T_2 weighted, although the contrast is due to the combined effects of chosen echo time, magnetization transfer, direct radio frequency saturation and diffusion as well as the T_1 and T_2 relaxation times of the tissue. The result is an excellent detailed visualization of anatomical structures, demonstrating the great potential of 4.7 T MRI for clinical applications. This paper shows that, with careful optimization of sequence parameters, FSE imaging can be used at high field to generate images with high spatial resolution and uniform contrast across the whole brain within the prescribed power deposition limits.

MRI systems utilizing high field magnets (3 T and above) have been available for a decade [1]. The advantages of higher magnetic field strength include increased MR signal-to-noise ratio (SNR) and increased sensitivity to blood oxygenation level dependent (BOLD) contrast, which is widely used for functional neuroimaging [2–4]. The increased spin-lattice relaxation time for blood makes the measurement of cerebral blood flow (CBF) by arterial spin labelling a more sensitive method at higher magnetic fields [5] and there are also attendant advantages to the performance of MR spectroscopy. The increased SNR, which varies approximately linearly with field strength, can theoretically be used to produce MR images with higher spatial resolution.

Conventional wisdom has suggested that the production of high-resolution images of the entire brain with uniform contrast behaviour may be confounded at high field by radiofrequency (RF) inhomogeneities. At magnetic field strengths of 3 T and higher the dielectric resonance effect and RF penetration issues [6] cause the flip angle to vary across the field of view (FoV) of the image. This produces spatial signal intensity variations and non-uniform contrast. For many MRI sequences, either the RF flip angle must be chosen as a compromise taking account of these variations, or specially shaped RF pulses must be employed that compensate for excitation pulse inhomogeneities [7] or are less sensitive to them (adiabatic pulses).

Fast spin echo (FSE) imaging [8, 9] (also known as turbo spin echo (TSE) or multishot rapid acquisition with relaxation enhancement (RARE)) is a method commonly used for the acquisition of diagnostic MRIs at clinical field strengths [10]. The FSE approach produces high quality images with contrast similar to that of conventional spin echo images and with the benefit of a greatly reduced acquisition time. Clinical applications of FSE include T_2 relaxometry and assessment of neurological disorders [11–14]. While the application of FSE imaging at high field is desirable, concerns exist regarding power deposition and image uniformity. It is probably for these reasons that other methods have been more commonly employed to generate structural brain images at high field strength [15–17].

The purpose of this paper is to demonstrate that, with accurate sequence optimization, FSE can be used to acquire good quality high resolution structural images of the human brain within practical examination times at high field strength. FSE images from a 4.7 T scanner are presented that display excellent contrast, spatial resolution and SNR.

Methods

Between August and November 2002, 10 healthy subjects (6 males, 4 females, age range 26–48 years, median age 30 years) were scanned with FSE after informed consent and approval from the University College London Hospital Ethics Committee. All imaging

Received 3 February 2003 and in revised form 1 May 2003, accepted 30 May 2003.

Address correspondence to Professor Roger Ordidge, The Wellcome Trust High Field MR Research Laboratory, Department of Medical Physics and Bioengineering, University College London, Shropshire House, 11–20 Capper Street, London WC1E 6JA, UK.

was performed using a 4.7 Tesla, 90 cm bore-diameter magnet (Magnex Scientific Ltd, Oxford, UK) controlled by a console supplied by Philips Medical Systems (Eindhoven, The Netherlands) based on a MR5000 design by SMIS Ltd (Guildford, UK). A shielded head gradient coil was used providing gradient fields of up to 36 mT m^{-1}. Images were acquired using a quadrature birdcage RF coil with an internal diameter of 28 cm. The FSE sequence had an echo train length of 8 echoes, with the first echo at 22 ms and an echo spacing of 22 ms. Sinc-shaped RF pulses were used for both signal excitation and refocusing, with relative amplitudes 1:1.8.

The repetition time (TR) was chosen either as 3.5 s for 17 slices or 7 s for 34 slices. Along the read axis, 512 points were acquired (sampling bandwidth 50 kHz) and 384 phase encoding (*pe*) steps were performed (with a factor of two oversampling) resulting in total acquisition times of 5 min 40 s (17 slices) or 11 min 20 s (34 slices). The slice thickness was 2 mm and the slice acquisition order was chosen to be either sequential with 2 mm gaps or interleaved with no gap between slices. In this way slices acquired consecutively in time were always at least 2 mm apart (to minimize slice interaction effects). The images presented here were acquired in axial and coronal orientations. For the axial images, a FoV of 240 mm × 180 mm (read axis × phase encoding axis) was chosen, resulting in an in-plane resolution of 469 μm × 469 μm. For the coronal images, a FoV of 200 mm × 200 mm was used (in-plane resolution: 391 μm × 521 μm). FSE imaging has also been performed with sagittal and oblique orientations (data not shown).

The specific absorption rate (SAR) for the FSE sequence with the above parameters was calculated to be below current safety limits of 4 W kg^{-1} for the head (for short exposure times [18]).

The nominal echo time (TE) corresponds to the time of acquisition of the central area of *k*-space [19] and was chosen either as 22 ms, 44 ms or 66 ms (corresponding to the 1st, 2nd or 3rd echo, respectively).

The exact scheme of *k*-space sampling has been shown to play a significant role in final image quality [9, 20]. The *k*-space coverage strategy in the *pe* direction was designed to ensure that when the data was combined prior to Fourier transformation (FT), signal intensity differences between echoes produced a relatively smooth amplitude variation through *k*-space. Therefore, the corresponding point spread function [19] did not contain significant sidebands and good image resolution was preserved. The 512 × 768 data matrix was zero-filled to 512 × 1024 and a Hanning filter [21] was applied along both directions prior to image reconstruction (FT). Due to the 2x oversampling in the *pe* direction, only the central portion of the image (a 512 × 512 matrix) was selected and stored. The final images were then obtained after filtering with SharpView™ [22], an image enhancement package currently installed on many clinical scanners.

Results

All 10 volunteers were successfully scanned with FSE. We illustrate our findings on FSE images from three subjects. Figure 1 shows four transverse sections from a 34-slice data set obtained on a 29-year-old male healthy volunteer with TE=22 ms. The images appear to be predominantly T_2 weighted with good grey-to-white matter (GM/WM) contrast. Figure 2 shows the same images displayed with an inverted grey scale (with Figure 2d showing an expanded region from Figure 1d). In these images blood vessels appear bright and are more clearly visible against surrounding dark background. Some details in the white matter are also more easily visible in these images including Virchow-Robin spaces (bright in conventional contrast and dark in inverted contrast, for example see arrows in Figure 2b). In the images of Figure 1b and 2b it is worth noting the appearance of the tail of the caudate nucleus (see arrows on Figure 2b). In Figures 1c and 2c the medullary laminae (arrow on Figure 2c) separating internal and external segments of the globus pallidus are also distinguishable. In Figures 1d and 2d the red nuclei and the substantia nigra appear hypo/hyperintense due to the effect of iron accumulation [23–25]. Fornices and mammillo thalamic tracts are also visible on the same images. Figures 3a and b show coronal sections from 17-slice data sets on two of the volunteers (male 30 years, TE=66 ms and female 34 years, TE=44 ms) with inverted grey scale. These images, as well as displaying excellent overall detail, allow easy discrimination of blood vessels and Virchow-Robin spaces. Figure 3a demonstrates good visualization of the internal capsule while in Figure 3b different layers of the hippocampus can be identified (alveus, cornu ammonis and gyrus dentatus, see arrows on Figure 3c). Despite the difference in TE the images display similar overall contrast. The GM/WM contrast is good and reasonably homogeneous in all the images shown.

Discussion

We have shown that with the correct choice of sequence and optimization of experimental parameters, T_2 weighted imaging can be performed with FSE at 4.7 T and displays the gain in quality expected from a high field system. Images with submillimetre in-plane resolution, high SNR and good structural contrast covering large brain regions can be produced in clinically acceptable acquisition times. Here we discuss particular features of our images and how they arise from the combination of tissue properties and sequence characteristics.

FSE images have a similar overall appearance to conventional T_2 weighted images. Clinically, FSE has replaced conventional spin echo imaging as the method of choice for diagnostic T_2 weighted imaging and T_2 relaxometry [11, 12]. At high field, T_2 values of brain tissue become shorter and more convergent than at 1.5 Tesla (63 ± 6 ms for cortical grey matter and 50 ± 2 ms for white matter at 4 T [26] *vs.* 91 ± 6 ms and 69–76 ms at 1.5 T [27]) and T_2 differences do not suffice to explain the contrast between grey and white matter seen in our images. This contrast can be explained by several other factors [9] such as the T_1 weighting introduced by the presence of stimulated echoes and the magnetization transfer effects.

In a multiecho spin-echo sequence comprising a train of refocusing pulses, the signal intensity decreases throughout the echo train due to T_2 relaxation. This signal decrease also depends strongly on flip-angle and therefore, due to RF inhomogeneity, will vary spatially resulting in signal non-uniformity across the image. In FSE, stimulated echoes compensate for the signal loss of the spin echoes,

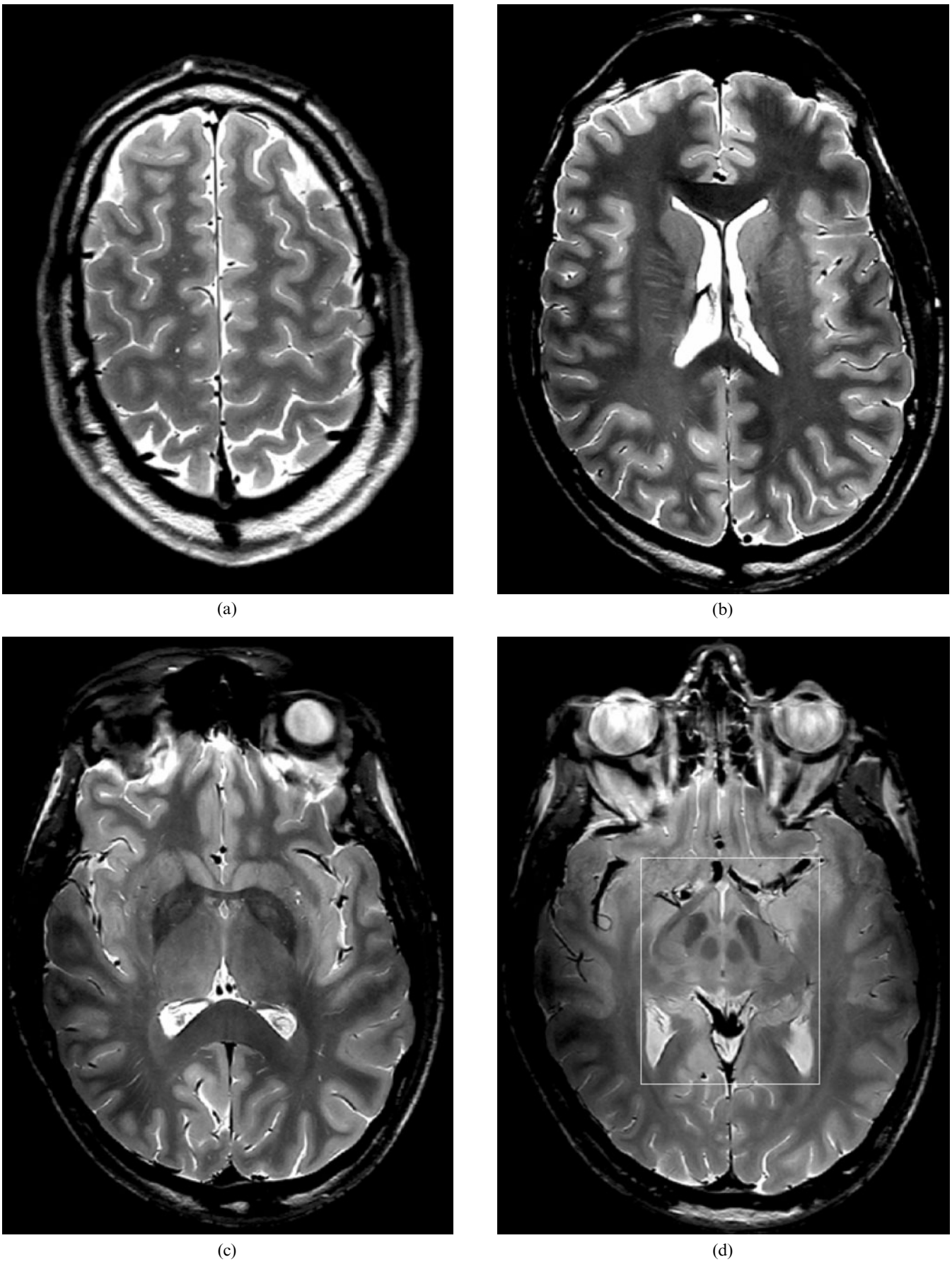

Figure 1. Fast spin echo high resolution transverse MRIs of a healthy volunteer (male, 29 years) displayed with conventional grey scale. Slice thickness 2 mm, in-plane resolution 469 μm × 469 μm, number of slices 34, total acquisition time 11 min 20 s. Figures (a) to (d) display four different sections from the top of the brain to the level of the substantia nigra. The white rectangle in Figure 1d indicates the region expanded in Figure 2d.

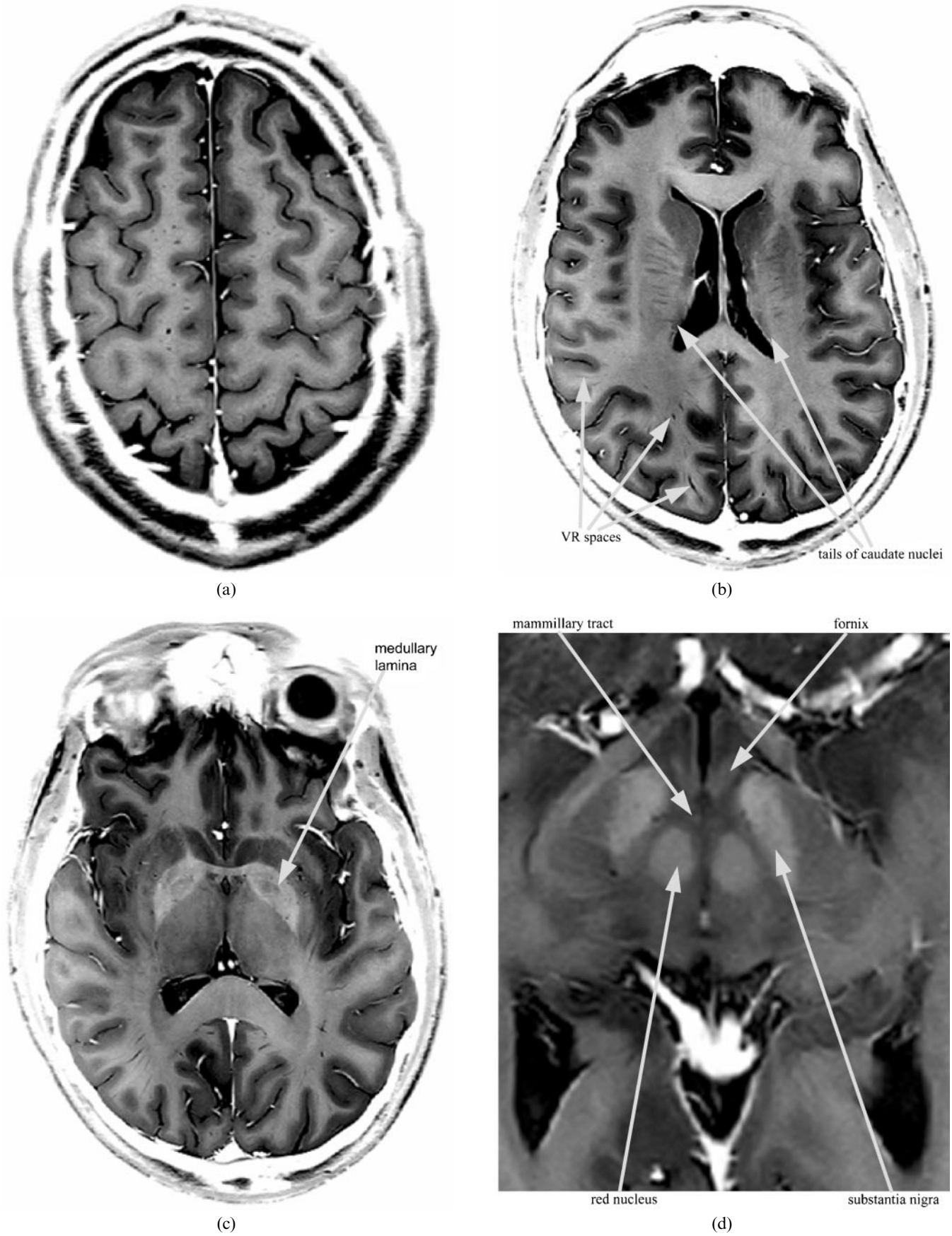

Figure 2. Same images as in Figure 1, presented with an inverted grey scale (with Figure 2d showing an expanded region from Figure 1d). Structures mentioned in the text are highlighted with grey arrows: tails of caudate nuclei and Virchow-Robin (VR) spaces (b); medullary lamina (c); fornix, mammillary tract, red nucleus and substantia nigra (d).

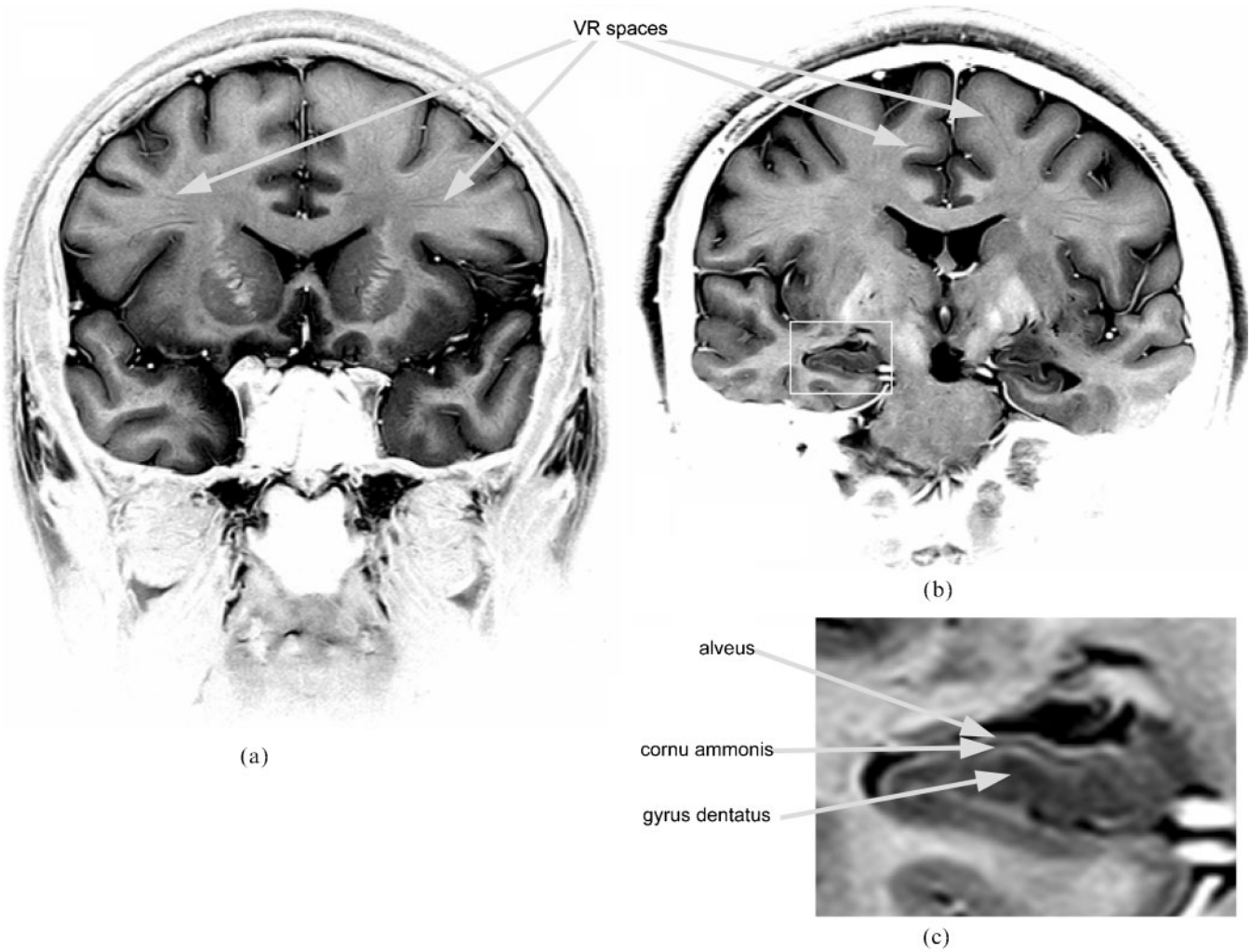

Figure 3. Fast spin echo high resolution coronal MRIs of (a) male, 30 years and (b) and (c) female, 34 years, displayed with an inverted grey scale. Slice thickness 2 mm, in-plane resolution 391 μm × 521 μm, number of slices 17, total acquisition time 5 min 40 s. Grey arrows indicate some of the readily visible Virchow-Robin (VR) spaces. The enlarged inset (c) from (b) shows the left hippocampus, with grey arrows indicating various internal structures (alveus, cornu ammonis, gyrus dentatus).

giving a degree of robustness to RF inhomogeneity, and the combined echo amplitude is dependent on T_1 as well as T_2 [28, 29]. At 4.7 T, the RF homogeneity within the brain is expected to be worse than at 1.5 T due to RF penetration and dielectric resonance effects [6]. However, the images shown here have relatively uniform signal intensity and contrast because of the aforementioned flip-angle insensitivity of FSE [30] in combination with the RF profile of a conventional birdcage coil.

Magnetization transfer (MT) effects [31], including both true MT and direct saturation, also contribute to the contrast in our images [16, 32]. These effects arise in the multislice FSE sequence because of the repetition of numerous refocusing pulses applied close to the resonance frequency of the imaged tissue during the aquisition of neighbouring planes [33]. Direct saturation affects grey and white matter by approximately equal amounts due to their similar T_1/T_2 ratios (~20 [26]). However MT increases contrast by preferentially attenuating myelinated tissue. The combination of T_2 weighting and MT may also account for the similar overall contrast observed for images acquired at different TE values [33].

Our images at 4.7 T were characterized by high contrast resolution as well as high spatial resolution resulting in excellent GM/WM contrast, good visualization of structures with high iron content and the identification of a high number of leptomeningeal blood vessels and Virchow-Robin spaces.

The GM/WM contrast appears to be good across all the slices. In addition a great deal of detail is visible in subcortical regions making the identification of anatomical structures, *e.g.* internal capsule, caudate nucleus, globus pallidus, medullary laminae, simpler than on equivalent images acquired at lower field strengths. Furthermore, it is interesting to note that the GM/WM contrast is enhanced when the volume coverage in the FSE sequence is increased. This is because the number of slices determines the minimum TR for a given resolution. For example the coronal 17-slice data sets shown in Figure 3 were acquired in 5 min 40 s (TR=3.5 s), while the axial data (Figures 1 and 2) covered 34 slices in twice the time (TR=7 s). The longer TR in the 34-slice sequence gives more time for longitudinal relaxation of the MR signal, resulting in a higher image SNR and better contrast.

Structures with high iron content such as the substantia nigra and red nuclei are also easily identifiable due to

their low signal in the FSE images. The increased iron concentration causes a reduction in T_2 relaxation time and this effect is enhanced at high magnetic fields [24, 25]. This iron-mediated contrast mechanism could allow the use of FSE for the investigation of movement disorders, where it is known that localized iron accumulation is abnormally high [34, 35].

Our images also allow easy identification of blood vessels within the cerebrospinal fluid (CSF) space (leptomeningeal vessels). This is due to the strong appearance of CSF, which has a long T_2 value, combined with the low signal intensity of intravascular blood. The scrambling of the spin phase of the blood due to in-plane flow results in incomplete rephasing of its signal prior to application of each refocusing RF pulse. Through-plane flow also causes blood signal dropout if spins move between slices during the echo train [36].

In addition, we have already mentioned the great number of identifiable Virchow-Robin spaces in our images. This number is remarkable with respect to 1.5 T observations, especially considering the relatively young age of the subjects whose images have been presented. One reason for this is the good contrast between Virchow-Robin spaces (characterized by high signal due to their fluid content) and the surrounding white matter (lower signal). Probably more important, however, is the higher spatial resolution of our FSE images compared with conventional images obtained at lower field.

While it is true that the spatial resolution of the images presented here is better than that of a standard clinical structural image, *e.g.* an FSE image obtained at 1.5 T in comparable time, higher resolution MR images acquired at 3 T and above have been published [17, 37, 38]. However, these studies have all focused on specific areas of the brain, mostly using RF receive coils of limited coverage and alternative methods to FSE. It was one of the aims of this study to investigate the potential of high resolution FSE as a method for whole brain imaging at 4.7 T using a conventional birdcage RF transmit/receive coil. The greater sensitivity associated with higher field strength does indeed allow the acquisition of high resolution images with a good SNR in clinically acceptable scan times.

Conclusions

In summary, we have demonstrated that with appropriate optimization of sequence parameters, the FSE technique can be used efficaciously at field strengths higher than 3 T and can deliver increased spatial resolution with useful tissue contrast across the whole brain within current safety limits.

Acknowledgments

We would like to thank The Wellcome Trust for support of this research.

References

1. Barfuss H, Fischer H, Hentschel D, Ladebeck R, Vetter J. Whole-body MR imaging and spectroscopy with a 4-T system. Radiology 1988;169:811–6.
2. Ogawa S, Lee TM, Kay AR, Tank DW. Brain magnetic resonance imaging with contrast dependent on blood oxygenation. Proc Natl Acad Sci USA 1990;87:9868–72.
3. Turner R, Le Bihan D, Moonen CT, Despres D, Frank J. Echo-planar time course MRI of cat brain oxygenation changes. Magn Reson Med 1991;22:159–66.
4. Bandettini PA, Wong EC, Hinks RS, Tikofsky RS, Hyde JS. Time course EPI of human brain function during task activation. Magn Reson Med 1992;25:390–7.
5. Wang J, Alsop DC, Li L, Listerud J, Gonzalez-At JB, Schnall MD, et al. Comparison of quantitative perfusion imaging using arterial spin labeling at 1.5 and 4.0 Tesla. Magn Reson Med 2002;48:242–54.
6. Hoult DI. Sensitivity and power deposition in a high-field imaging experiment. J Magn Reson Imaging 2000;12:46–67.
7. Deichmann R, Good CD, Turner R. RF inhomogeneity compensation in structural brain imaging. Magn Reson Med 2002;47:398–402.
8. Hennig J, Nauerth A, Friedburg H. RARE imaging: a fast imaging method for clinical MR. Magn Reson Med 1986;3:823–33.
9. Constable RT, Anderson AW, Zhong J, Gore JC. Factors influencing contrast in fast spin-echo MR imaging. Magn Reson Imaging 1992;10:497–511.
10. Kiefer B. Turbo spin echo imaging. In: Schmitt F, Stehling MK, Turner R, editors. Echo planar imaging. Theory, technique and applications. Berlin: Springer 1998:583–604.
11. Woermann FG, Steiner H, Barker GJ, Bartlett PA, Elger CE, Duncan JS, et al. A fast FLAIR dual-echo technique for hippocampal T_2 relaxometry: first experiences in patients with temporal lobe epilepsy. J Magn Reson Imaging 2001; 13:547–52.
12. von Oertzen J, Urbach H, Blumcke I, Reuber M, Traber F, Peveling T, et al. Time-efficient T_2 relaxometry of the entire hippocampus is feasible in temporal lobe epilepsy. Neurology 2002;58:257–64.
13. Tomura N, Kato K, Takahashi S, Sashi R, Sakuma I, Narita K et al. Comparison of multishot echo-planar fluid-attenuated inversion-recovery imaging with fast spin-echo fluid-attenuated inversion-recovery and T_2 weighted imaging in depiction of white matter lesions. J Comput Assist Tomogr 2002;26:810–4.
14. Hirabayashi H, Tengvar M, Hariz MI. Stereotactic imaging of the pallidal target. Mov Disord 2002;17 Suppl. 3:130–4.
15. Lee JH, Garwood M, Menon R, Adriany G, Andersen P, Truwit CL, et al. High contrast and fast three-dimensional magnetic resonance imaging at high fields. Magn Reson Med 1995;34:308–12.
16. Duewell S, Wolff SD, Wen H, Balaban RS, Jezzard P. MR imaging contrast in human brain tissue: assessment and optimization at 4 T. Radiology 1996;199:780–6.
17. Chakeres DW, Abduljalil AM, Novak P, Novak V. Comparison of 1.5 and 8 tesla high-resolution magnetic resonance imaging of lacunar infarcts. J Comput Assist Tomogr 2002;26:628–32.
18. Medical Devices Agency. Guidelines for magnetic resonance equipment in clinical use. London, UK: MDA 2002.
19. Liang Z-P, Lauterbur PC. Principles of magnetic resonance imaging. A signal processing perspective. New York: IEEE Press, 2000.
20. Mulkern RV, Wong ST, Winalski C, Jolesz FA. Contrast manipulation and artifact assessment of 2D and 3D RARE sequences. Magn Reson Imaging 1990;8:557–66.
21. Press WH, Flannery BP, Teukolsky SA, Vetterling WT. Numerical recipes in C. The art of scientific computing. Cambridge: Cambridge University Press, 1988.
22. Image enhancement package. ContextVision, www.contextvision.se. Sweden.
23. Drayer B, Burger P, Darwin R, Riederer S, Herfkens R, Johnson GA. MRI of brain iron. AJR Am J Roentgenol 1986;147:103–10.

24. Ordidge RJ, Gorell JM, Deniau JC, Knight RA, Helpern JA. Assessment of relative brain iron concentrations using T_2 weighted and T_2*-weighted MRI at 3 Tesla. Magn Reson Med 1994;32:335–41.
25. Schenck JF. Imaging of brain iron by magnetic resonance: T_2 relaxation at different field strengths. J Neurol Sci 1995;134 (Suppl.):10–8.
26. Jezzard P, Duewell S, Balaban RS. MR relaxation times in human brain: measurement at 4T. Radiology 1996;199:773–9.
27. Breger RK, Rimm AA, Fischer ME, Papke RA, Haughton VM. T_1 and T_2 measurements on a 1.5-T commercial MR imager. Radiology 1989;11:273–6.
28. Hennig J. Echoes—how to generate, recognize, use or avoid them in MR-imaging sequences. Conc Magn Reson 1991; 3:125–43.
29. Williams CF, Redpath TW, Smith FW. The influence of stimulated echoes on contrast in fast spin-echo imaging. Magn Reson Imaging 1996;14:419–28.
30. Alsop DC. The sensitivity of low flip angle RARE imaging. Magn Reson Med 1997;37:176–84.
31. Balaban RS, Ceckler TL. Magnetization transfer contrast in magnetic resonance imaging. Magn Reson Q 1992;8:116–37.
32. Henkelman RM, Stanisz GJ, Graham SJ. Magnetization transfer in MRI: a review. NMR Biomed 2001;14:57–64.
33. Melki PS, Mulkern RV. Magnetization transfer effects in multislice RARE sequences. Magn Reson Med 1992;24:189–95.
34. Martin WR. Magnetic resonance imaging and spectroscopy in Parkinson's disease. Adv Neurol 2001;86:197–203.
35. O'Neill J, Schuff N, Marks WJ Jr, Feiwell R, Aminoff MJ, Weiner MW. Quantitative 1H magnetic resonance spectroscopy and MRI of Parkinson's disease. Mov Disord 2002;17:917–27.
36. Wehrli FW, Bradley WG. Magnetic resonance flow phenomena and flow imaging. In: Biomedical magnetic resonance imaging principles, methodology and applications. Wehrli FW, Shaw D, Kneeland JB, editors. New York: VCH Publishers Inc, 1988.
37. Clare S, Jezzard P, Matthews PM. Identification of the myelinated layers in striate cortex on high resolution MRI at 3 Tesla. In: Proc. 10th Annual Meeting ISMRM, Hawaii, USA, May Berkley, CA: ISMRM, 2002:1465.
38. Barbier EL, Marrett S, Danek A, Vortmeyer A, van Gelderen P, Duyn J, et al. Imaging cortical anatomy by high-resolution MR at 3.0T: detection of the stripe of Gennari in visual area 17. Magn Reson Med 2002;48:735–8.